Proceedings of 4th International Conference on Trends in Welding Research, Gatlinburg TN, June 1995

Modeling and Validation of Residual Stress Distribution in an HSLA-100 Disk

Z. Feng*, Y.Y. Zhu*, T. Zacharia*, R.J. Fields**, P.C. Brand***, H.J. Prask** and J.M. Blackburn****

* Oak Ridge National Laboratory, Oak Ridge TN
** National Institute of Standards and Technology (NIST), Gaithersburg, MD
*** University of Maryland, College Park MD; Guest Researcher at NIST
**** Navy Surface War Center, Annapolis, MD

Abstract

The residual stress distribution in a GTA spot welded HSLA-100 steel disk was analyzed using thermomechanically uncoupled and semi-coupled finite element (FE) formulations and measured with the neutron diffraction technique. The computations used temperature-dependent thermophysical and mechanical properties of the base metal. The thermal analysis was based on the heat conduction formulation with the Gaussian heat input from the arc. The semi-coupled approach is an effective alternative to the fully coupled approach in which the incompatibility in the thermal and mechanical time increments often leads to numerical convergence difficulties. Convergence was achieved in the semi-coupled approach where a larger time increment for temperature calculation was automatically divided into some sub-intervals for the thermal stress calculation. The temperature, deformation configurations, and state variables were updated at the end of the temperature increment.

The predictions from the FE models are in very good agreement with the neutron measurement results in the far heat-affected zone (HAZ) and in the base metal. Both models over-predicted the residual stress field in the fusion zone and near HAZ as measured by the neutron diffraction method. The discrepancy could be attributed to the changes in microstructures and material properties in the HAZ and fusion zone due to phase transformations during the welding thermal cycle. The formation of cracks in the fusion zone is another factor that possibly contributes to the lower measured residual stress values.

Residual stresses develop in a material during welding due to the uneven distribution of inelastic strains caused by the localized heating from the welding heat source and the subsequent uneven cooling of the material. Solidification shrinkage of the weld metal and local thermal expansion and contraction are the common causes for welding residual stresses in engineering materials. For alloys that experience solid state phase transformations during welding, the transformation plasticity and volumetric changes accompanied with the transformations are additional contributing factors (1). The magnitude and distribution of welding residual stress are also influenced by the material property changes (yield strength, for example) caused by the welding thermal cycles and the use of different filler metals.

The formation of welding residual stresses is a thermo-mechanical-metallurgically coupled phenomenon. The temperature distribution, microstructure and stress/strain relationships change in a complicated manner during the course of welding due to complex interaction between them. It is extremely difficult to develop fully coupled modeling methods for the welding residual stress calculation. It requires a thorough knowledge of the thermal, mechanical, and phase transformation phenomena and their interactions. In the past, researchers have tried to separate these coupling effects in welding residual stress modeling. In some alloy systems, their effects indeed can be uncoupled. For example, many austenitic stainless steels do not experience solid state phase transformation during welding. Thus the metallurgical effects can be readily ignored (uncoupled) from the thermo-mechanical models for these alloys. As to the thermo-mechanical coupling, it is the common opinion that the coupling can be regarded as only a one-way process, that is, the mechanical responses of a weldment do not strongly influence its thermal behavior during the course of welding (2). Therefore, the majority of modeling work on the residual stresses and distortions of welded structures take the thermomechanically uncoupled approach (3-5). There also have been a few thermo-mechanically coupled studies in the past (6,7). However, there are seldom direct comparisons of the calculation results between thermomechanically uncoupled and coupled models.

HSLA-100 is a very low carbon, fine grained steel additionally strengthened by copper precipitation (8). The

alloying elements make HSLA-100 highly hardenable. Therefore, it is possible to form martensite and bainite in the HAZ and autogenous weld metal under normal welding conditions (9). The formation of martensite and bainite phases during welding produces microstructures in the HAZ and fusion zone that have significantly different mechanical properties from those of the base metal, in addition to the transformation plasticity effects. There are no well developed modeling procedures to reliably predict the residual stresses in the weldment of HSLA-100 steels. For example, there are no existing models to quantitatively relate the yield strength in the HAZ to the variations of welding conditions, although there have been many recent attempts to relate the microstructural changes to welding conditions.

In this study, the residual stress in a HSLA-100 steel disk was analyzed by FE models and experimentally determined by neutron diffraction. Both thermomechanically uncoupled and semi-coupled FE approaches are applied to the same weldment. The purpose is to determine whether or not the different FE formulations would result in any differences in predicting the residual stresses during welding. The use of the same weldment allows for direct comparison of the modeling methods. The microstructural changes in the HAZ and fusion zone are not included in this stage, in an attempt to provide the baseline information for an on-going model development that will eventually include all the thermo-mechanical-metallurgical coupling effects.

Welding Parameters

Miller CC/CP 1500	5 second welding time
4 mm diameter electrode	5 second post purge
320 amps	Argon shielding
15 volts	40 - 45 CFH

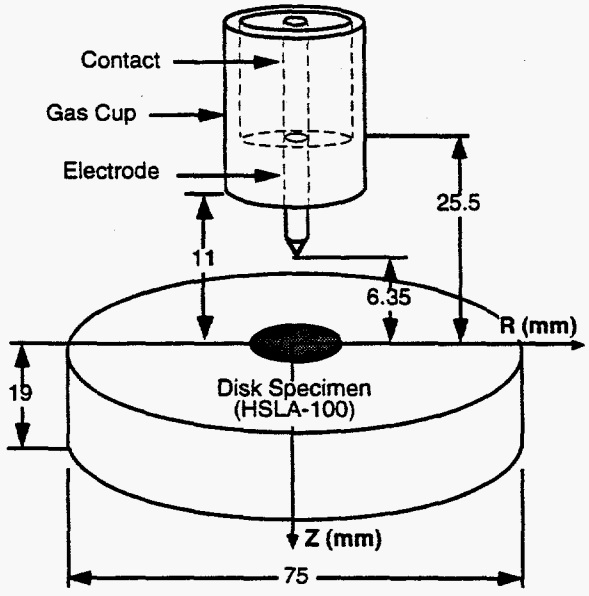

Figure 1 Welding setup.

Experimental

Welding and Material Detail. The base metal used for welding was HSLA-100 steel with a nominal yield strength of 690 MPa at the ambient temperature. The chemical composition is given in Table I.

Table I. Chemical composition of material (Wt%)

C	Mn	P	S	Si	Cu	Ni	Cr	Mo	Al	Nb
.04	.84	.006	.002	.25	1.6	3.48	.56	.57	.028	.027

An autogenous spot weld was made on a HSLA-100 steel disk using gas tungsten arc welding process without filler metal (Figure 1). The disk was measured 19 mm (3/4") in height and 75 mm (3") in diameter. The weld was located at the center of the top surface of the disk and produced with the following welding parameters: 320A, 15V, 5 second arc time and a 4 mm (5/32") diameter electrode. The welding was shielded with argon and followed by a 5 second post purge. No constraint (fixture) was used during welding and subsequent cooling.

Neutron Diffraction Measurement. Neutron Diffraction Measurement were performed on the Beam Tube-6 (BT-6) triple-axis spectrometer at the National Institute of Standard and Technology (NIST) Research Reactor. Instrumental details and measurement methodology have been discussed elsewhere (10,11). The measurement was made using a nominal gauge volume of 3 x 3 x 3 mm. Figure 2 illustrates the positions and relative size of the measurement points which are located on a radial section plane.

Computational Model

The finite element models were constructed according to the above experimental essentials. The highly desirable symmetry of welding and experimental design enabled the use of two-dimensional axisymmetric simplification in the analysis. The axisymmetric plane was discretized with about 450 second-order 8-node quadrilateral elements with a reduced integration scheme for the mechanical calculation. Compatible elements were used for the thermal calculation. Finer meshes

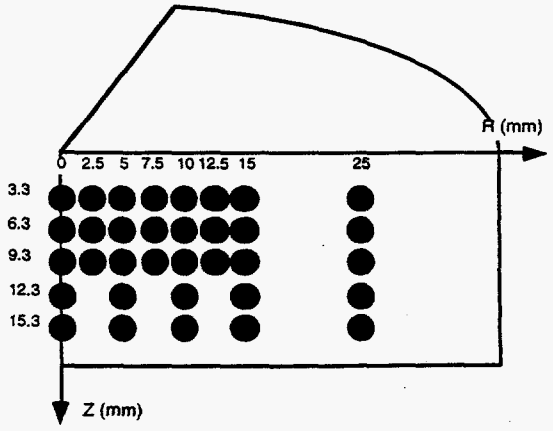

Figure 2 Neutron diffraction measurement locations

were generated in the weld and the surrounding areas.

Two different FE formulations were used. The first one was a thermomechanically semi-coupled formulation. The second one was based on the thermomechanically uncoupled approach. The only difference between the two methods was the formulation of the thermomechanical coupling effect.

In the thermomechanically uncoupled formulation, the heat transfer analysis was decoupled from the mechanical analysis. The solution process was in principle similar to those commonly used in FE analyses of welding residual stress and distortion problems (2,4) . The temperature history of the model was calculated according to the original geometrical configuration of the disk, independent from the mechanical analysis. The thermal history of the model was then used as a thermal load in the subsequent mechanical calculation.

The thermomechanically semi-coupled formulation was a derivation of the fully coupled approach (12,13). The objective was to circumvent the incompatible time increment problem that is commonly encountered in the thermal and mechanical calculations during the course of welding.

According to our experience, it is usually very difficult to perform fully coupled thermomechanical calculations of welding residual stresses and distortions. The problem results from the different requirements for the thermal and mechanical time increments. It is well known that, in the transient heat transfer analysis based on the conduction formulation, there is a minimum usable time increment below which the system tries to keep a global enthalpy response and spatial oscillations may appear. The following formula gives a general idea of this critical time increment for the implicit integration scheme (14):

$$\Delta t \geq \frac{\rho C_p}{6\kappa}(\Delta l)^2$$

where K is the thermal conductivity, ρC_p the heat capacity, Δt the time increment and Δl the element size. It is only approximate in nonlinear thermal analysis, because it is defined for linear systems and a precise temporal integration scheme. With the average values of thermophysical properties of low carbon steels (K = 30 W/m-K, $\rho C_p = 6\text{x}10^6$ J/m^3-K), the above equation indicates that the time increment for an element size of 2 mm should be greater than 0.1 second.

On the other hand, even for a problem with a rate-independent stress-strain constitutive relation, the fully coupled thermomechanical analysis becomes rate-sensitive owing to the transient, time dependent temperature field. From our attempts on welding simulation using thermo-elastoplastic laws, the maximum time increment required for convergent mechanical calculations can be easily less than 0.01 second. This means that the fully coupled thermomechanical analysis needs very fine element sizes that are computationally prohibitive for a practical welded structure. Otherwise, the time increment in the mechanical calculations will not guarantee the correct result for the temperature field. Therefore, a semi-coupled formulation was used in this study. The idea is to (1) divide the total welding time into some "parent" time increments that are suitable for the thermal analysis, and perform thermal calculation for one parent increment; (2) divide the thermal parent increment into several sub-increments according to an automatic scheme based on stress convergency considerations, linearly interpolate the temperature data of the parent increment onto the sub-increments, and perform the mechanical calculation in each of the sub-increments; (3) update the temperature, deformation configuration and state variables at the end of the parent increment; (4) go to the next parent increment.

Temperature dependent thermophysical properties were used in this study. The thermal conductivity above the melting temperature was artificially increased to compensate for the convective heat transfer effect. The energy input from the welding arc to the disk's surface took the form of a Gaussian distribution (surface heat flux), with a characteristic arc radius of 6.0 mm. The use of this rather large arc radius was related to the unusually high welding current used in the test.

Temperature-dependent, rate-independent elasto-plastic constitutive equations were constructed from the uniaxial tensile testing results of the base metal as determined under various temperature and strain rate conditions. Properties were extrapolated for temperatures above 1300K. The effects of microstructural changes in the fusion zone and HAZ were not included in the model.

Results

Figure 3 shows the Von Mises stress contours from the two different FE formulations. Von Mises stress is chosen because

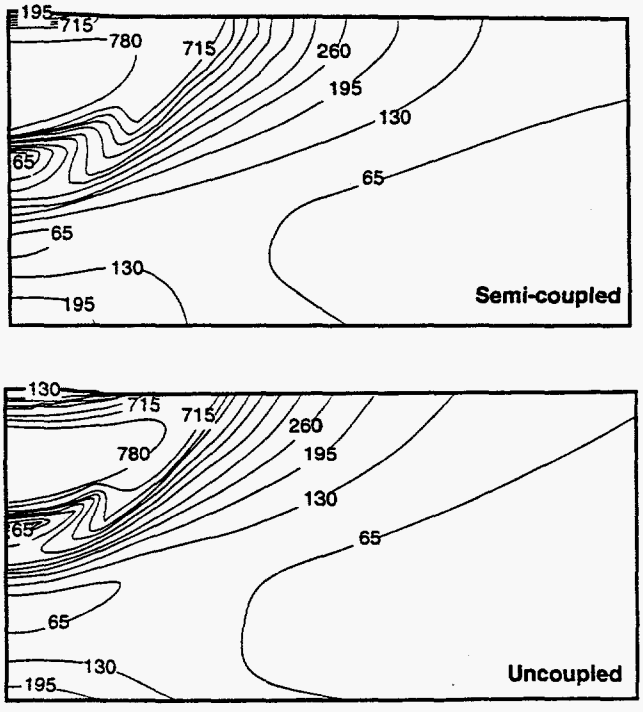

Figure 3 Von Mises stress distributions as calculated from two different FE formulations, stresses are in MPa.

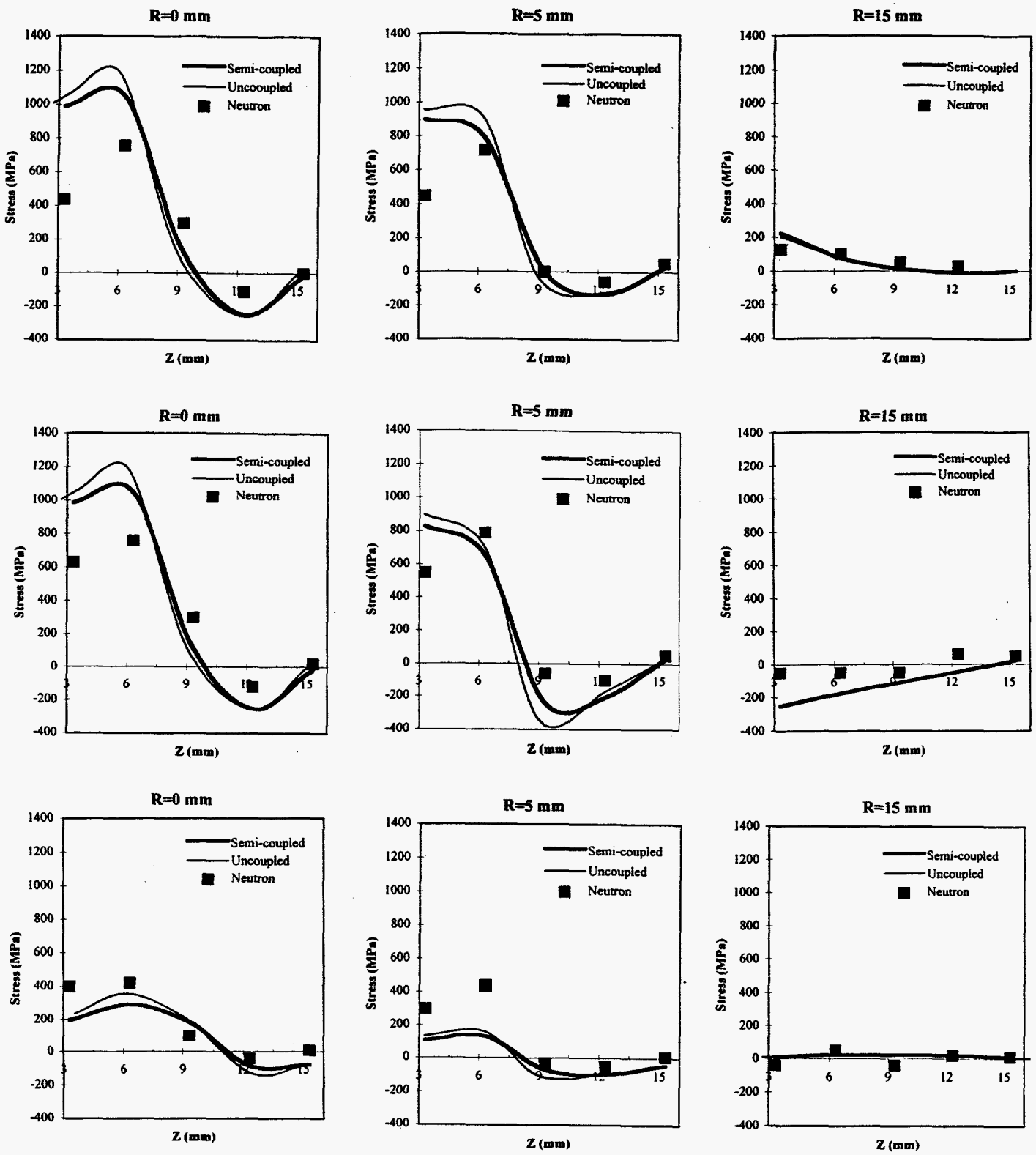

Figure 4 Comparison of neutron measurement and FEM predictions. Top: Radial stress, Middle: Hoop stress, and Bottom: Axial stress

it represents the overall effect of all stress components. It is clear that the overall Von Mises stress distributions are very similar for the two formulations. However, there are some differences in the stress magnitudes in a few localized regions.

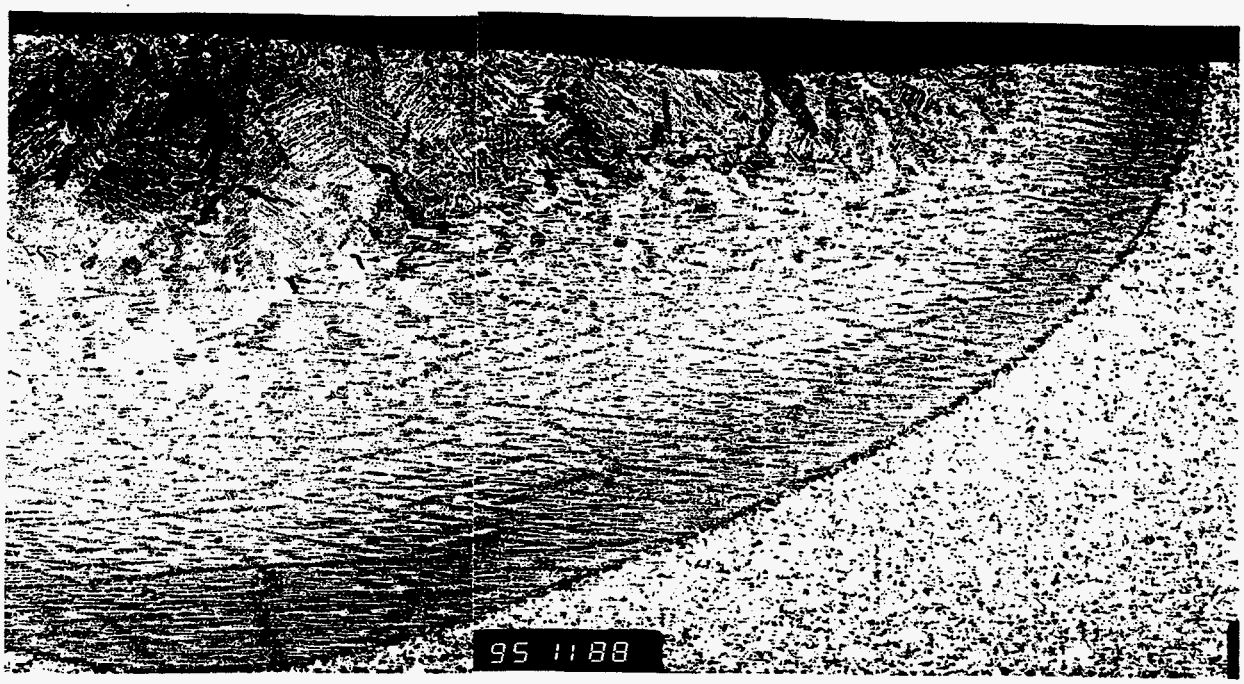

Figure 5 Microstructures and cracks in the fusion zone, magnification: x13

Comparisons between the neutron diffraction measurement results and the FE predictions are shown in Figure 4 in which the residual stresses are plotted as functions of the distance from the weld surface (the Z direction in Figure 1). Comparisons of all three normal stress components are made at three radial distances (R=0, 5 and 15 mm) from the weld centerline. Predictions from both FE formulations are presented in the figures. Again, calculations from the two FE codes are very close to each other. Both of them are able to predict the essential characteristics of residual stress patterns in the disk as obtained from the neutron diffraction measurement. It is hard to tell which FE model is more appropriate, based on the comparison with the measurement results. The predictions are in very good agreement with the neutron measurement results in the far HAZ and base metal. However, in the near HAZ and fusion zone, predictions from both models are higher than those measured. The causes for the discrepancies between prediction and measurement in the fusion zone and HAZ can be complicated. One of the reasons is the microstructural changes in the fusion zone and near HAZ that took place during welding. The microstructure in the disk prior to welding was a fine grained bainite plus copper precipitates, with hardness of about 25 HRC. Because of the high hardenability of HSLA-100, the fusion zone and near HAZ transformed to a much harder microstructure of mixed untempered martensite and bainite (about 35 HRC). Figure 5 shows the microstructure changes in the fusion zone and HAZ. Another source of discrepancy may be associated with the fact that the neutron measurements average over 3x3x3 mm^3 volume element. This tends to blur the actual distribution, particularly in the area where the stress gradient is high.

The microstructure changes in the fusion zone and HAZ of HSLA-100 have two opposite effects on the residual stress levels that were not considered in the model. The first one is the increased yield strength in the fusion zone and HAZ, as indicated by the changes in hardness. The higher yield strength tends to increase the residual stress level in the fusion zone and HAZ since these areas experience plastic deformation according to the calculation. On the other hand, martensite phase transformation is accompanied with a volume expansion that partially diminishes the thermal contraction. This effect tends to reduce the residual stress levels in the fusion zone and HAZ.

Perhaps an unexpected factor is cracking of fusion zone during or shortly after welding. As shown in Figure 5, a number of cracks were formed beneath the weld surface in the fusion zone. The size of the cracks ranges from less than 0.1 mm to about 2 mm. Obviously, the formation of these cracks relaxed the residual stress levels around them. However, the randomly distributed cracks made it very difficult to accurately simulate all the cracks in the FE models. As a first estimate, only one crack was introduced into the uncoupled FE models when the weld metal begins to cool down from 1500K. This was to simulate the effect of a solidification crack on the residual stress distribution.

The location of the crack was chosen to represent the longest crack in Figure 5 indicated by the arrow. The crack was parallel to the axial (Z) direction, about 1 mm from the axial axis of the disk. It was 2 mm long, with the near crack tip about 1.5 mm from the weld surface. Figure 6 shows the effect of the crack on the hoop residual stress distribution. As expected, the residual stress levels around the crack are significantly reduced. Surprisingly, the reduction is very localized. The

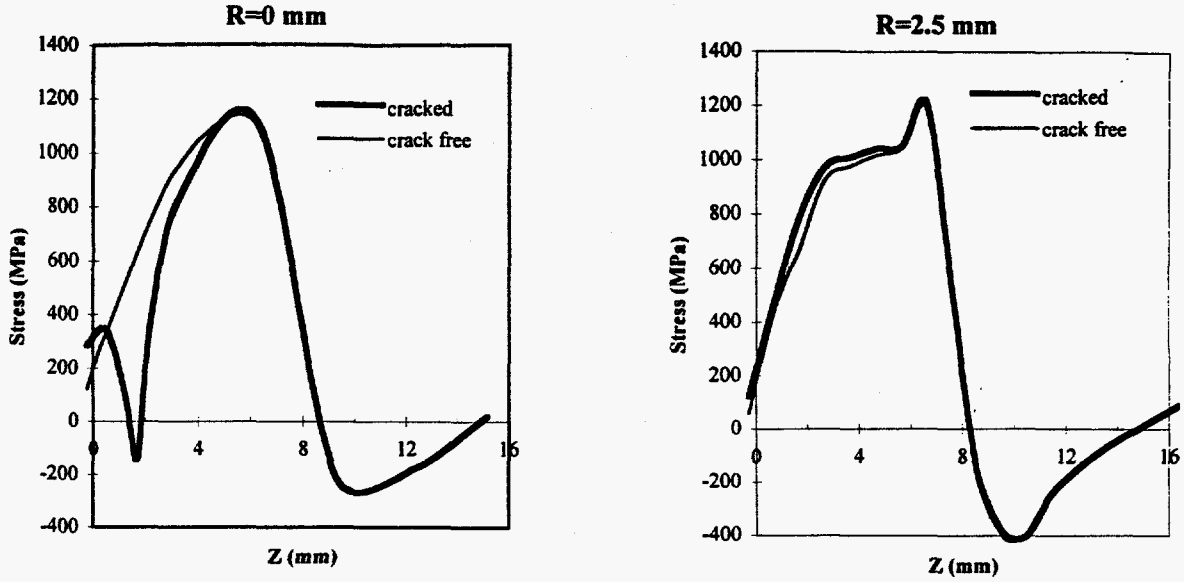

Figure 6 Effect of a single crack on the hoop residual stress distributions, uncoupled formulation

effects of the introduced crack begin to diminish at a distance of merely 2.5 mm from the weld centerline (R=2.5 mm). This implies that the cracks in the fusion zone may not significantly change the residual stress levels in the base metal and far HAZ, which is consistent with the comparisons between the measurement and modeling results.

Conclusions

(1) There are some differences in the predicted residual stress levels in the HSLA-100 steel disk, when the results from the thermomechanically uncoupled and semi-coupled FE formulations are compared. However, these differences are relatively small. The neutron diffraction measurement could not differentiate which model is more appropriate.

(2) The predictions from both FE models show very good agreement with the neutron diffraction measurement results in the regions away from the fusion zone.

(3) Both FE models over-predict the residual stresses measured in the fusion zone and near HAZ. The discrepancy could be attributed to the changes in microstructures and mechanical properties in the fusion zone and HAZ. The formation of cracks in the fusion zone is another factor that possibly contributes to the lower measured residual stress levels.

(4) Preliminary FE analysis indicates that the effect of cracks on the relaxation of residual stresses are localized to the region around the cracks. Therefore, it is possible that the residual stress predications in the base metal and far HAZ are not greatly affected by the cracks.

Acknowledgment

The authors thank Drs. S. Babu and S. Simunovic of Oak Ridge National Laboratory for reviewing of this paper. This research is sponsored by the U.S. Navy, Office of Naval Research under interagency agreement DOE No. 1866-E126-AI, Navy No. N00014-92-F-00639 under Department of Energy contract No DE-AC05-84OR21400 with Lockheed Martin Energy Systems, and by appointment to the Oak Ridge National Laboratory Postdoctoral Research Associates Program administrated jointly by the Oak Ridge Institute for Science and Education and Oak Ridge National Laboratory.

References

1 Leblond, J.B., G. Mottet, and J.C. Devaux. J. Mech. Phys. Solids 1986 34(4) 395-432.
2 Hibbitt, H.D. and P.V. Marcal. Computers & Structures, 1990, 1145-1174.
3 Friedman, E. J. Pressure Vessel Tech. 97 Series J (3) 1975, 206-213.
4 Shim, Y. Z. Feng, S. Lee, D.S. Kim, J. Jaeger, J.C. Paparitan and C.L. Tsai. Welding J. (9) 1992, 305s-312s.
5 Karlsson, R.I. and B.L. Josefson. J. Pressure Vessel Tech. vol 112 (3) 1990, 76-84.
6 Argyris, J.H., L.E. Vaz and K.J. William, J. Thermal Stresses, (4) 1981, 121-153.
7 Mahin, K.W., W. Winters, T.M. Holden, R.R. Hosbous, and S.R. MacEwen. Welding J. (9) 1991, 245s-260s.
8 Czyryca E.J. Int. Conf. on Metall., Welding and Qualification of Microalloyed (HSLA) Steel Weldments, (Preprint) Nov 6-8 1990, Houston TX, 549-568.
9 Smith, N.J., J.T. McGrath, J.T. Bowker and J.A. Gianeto. Int. Conf. on Metall., Welding and Qualification of Microalloyed (HSLA) Steel Weldments, (Preprint) Nov 6-8 1990, Houston TX, 306-324.
10 Prask, H.J. and C.S. Choi. Practical Applications of Residual Stress Technology, (ed. C. Ruud), ASM International, Metals Park, OH 1991, 87-93.
11 Brand, P.C., H.J. Prask, J. Blackburn, R.J. Fields, and T.M. Proctor. Proc. 1994 MRS Fall Meeting in Boston (in press).
12 Three-dimensional Finite Element Analysis for Welding Processes, Internal Report of ORNL, 1994.
13 Zhu, Y.Y. and S. Cescotto, Computers & Structures, Vol.53, 1994, 275-304.
14 ABAQUS/Standard User's Manual Version 5.4. Hibbitt, Karlsson & Soreness, Inc., Pawtucket, RI. 1994.

DISCLAIMER